https://doi.org/10.5194/acp-2021-302
Preprint. Discussion started: 1 July 2021

Atmospheric Chemistry and Physics Discussions

Methodology to determine the coupling of continental clouds with surface from lidar and meteorological data

Tianning Su[1], Youtong Zheng[1], and Zhanqing Li[1]

[1]Department of Atmospheric and Oceanic Sciences & ESSIC, University of Maryland, College Park, Maryland 20740, USA

Correspondence to: zhanqing@umd.edu; tianning@umd.edu

https://doi.org/10.5194/acp-2021-302
Preprint. Discussion started: 1 July 2021

Atmospheric Chemistry and Physics Discussions

Abstract

The states of coupling between clouds and surface or boundary-layer have been investigated much more extensively for marine stratocumulus clouds than for continental low clouds, partly due to more complex thermodynamic structures over land. A manifestation is a lack of robust remote sensing methods to identify coupled and decoupled clouds over land. Here, we have generalized the concept of coupling and decoupling to low clouds over land, based on potential temperature profiles. Furthermore, by using ample measurements from a lidar and a suite of surface meteorological instruments at the U.S. Department of Energy's Atmospheric Radiation Measurement Program's Southern Great Plains site from 1998 to 2019, we have developed a method to simultaneously retrieve the planetary boundary layer (PBL) height (PBLH) and coupled states under cloudy conditions during the daytime. The coupled states derived from lidar show strong consistency with those derived from radiosondes. Retrieving the PBLH under cloudy conditions that has been a persistent problem in lidar remote sensing, is resolved in this study. Our method can lead to high-quality retrievals of the PBLH under cloudy conditions and the determination of cloud coupling states. With the new method, we find that coupled clouds are sensitive to changes in the PBL with a strong diurnal cycle, whereas decoupled clouds and the PBL are weakly related. Since coupled and decoupled clouds have distinct features, our new method offers an advanced tool to separately investigate them in climate systems.

https://doi.org/10.5194/acp-2021-302
Preprint. Discussion started: 1 July 2021


Atmospheric Chemistry and Physics Discussions

1 Introduction

A large fraction of low clouds is driven by surface fluxes through the conduits of the planetary boundary layer (PBL) over land (e.g., Betts, 2009; Ek and Holtslag, 2004; Golaz et al., 2002; Teixeira and Hogan, 2002; Zheng et al., 2020; Wei et al., 2020; Santanello et al., 2018). This is a coupled cloud-surface system (Cheruy et al., 2014; Zheng & Rosenfeld, 2015; Wu et al., 1998). However, not all low clouds respond to surface forcing. Those clouds without close interactions with the local surface are considered to be in a decoupled state. Given that the PBL is, by definition, the lowest atmospheric layer influenced by the underlying surface (Stull, 1988), to what degree the PBL top overlaps with cloud bases becomes a good criterion to separate coupled and decoupled low clouds.

Conventionally, the "coupled state" of a cloud-topped marine boundary layer implies that the moist conserved variables are vertically well mixed within the PBL (Bretherton and Wyant, 1997; Dong et al., 2015; Zheng & Li, 2019; Zheng et al., 2018). However, such a definition cannot be simply applied to clouds over land since the moist conserved variables typically show considerable variations due to the relatively complex thermodynamics (Driedonks, 1982; Stull, 1988). The definition and the determination methods of the PBL over land also widely differ from those over ocean (Garratt, 1994; Vogelezang & Holtslag, 1996). The concept of coupled and decoupled states is typically used to characterize marine stratocumulus clouds due to their large-scale coverages (Nicholls, 1984). Since stratocumulus only constitutes a relatively small portion of continental clouds (Warren et al., 1986), we attempt to

https://doi.org/10.5194/acp-2021-302
Preprint. Discussion started: 1 July 2021


Atmospheric Chemistry and Physics Discussions

extend the concept of coupling and decoupling to characterize low clouds over land.

Following parcel theory, the lifted condensation level (LCL) has been used to diagnose a coupled cloud, based on the distance between the LCL and the cloud base (e.g., Dong et al., 2015; Glenn et al., 2020; Zheng & Rosenfeld, 2015; Zheng et al., 2020). When potential temperature and humidity are uniformly distributed in the vertical, the LCL should be consistent with the cloud base for coupled cases. However, the cloud base for coupled cases can considerably differ from the LCL over land because potential temperature and humidity have large variabilities in the vertical scale within the PBL over land (Guo et al., 2016; Stull, 1988; Su et al., 2017a). Therefore, a robust remote sensing method is still warranted to distinguish coupled and decoupled clouds over land.

Since the PBL height (PBLH) is the maximum height directly influenced by surface fluxes, we consider coupling with the PBL equivalent to coupling with the land surface. Thus, we use the PBLH as a critical parameter to diagnose the coupling between clouds and the land surface. The degree of coupling may thus be gauged in terms of quantitative differences between the cloud base and the PBL top. Such differences can be determined in a height coordinate system or in a potential temperature coordinate system (Kasahara, 1974). For this purpose, ground-based lidar has great potential because it can continuously track the development of the PBL (Demoz et al., 2006; Hageli et al., 2000; Sawyer & Li, 2013; Su et al., 2017b) and clouds (Clothiaux et al., 2000; Platt et al., 1994; Zhao et al., 2014) at high temporal and vertical resolutions.

https://doi.org/10.5194/acp-2021-302
Preprint. Discussion started: 1 July 2021


Atmospheric Chemistry and Physics Discussions

By jointly using lidar measurements and meteorological data from the U.S. Department of Energy's Atmospheric Radiation Measurement (ARM) Southern Great Plains (SGP) site (36.6°N, 97.48°W), we attempt to identify coupled and decoupled low clouds during the daytime. Unlike previous studies that use the LCL or radiosonde (RS) data to diagnose coupled clouds (e.g., Dong et al., 2015; Zheng & Rosenfeld, 2015), this study provides the first lidar-based method to automatically determine the coupling and decoupling of low clouds over land at a high temporal resolution.

The paper is organized as follows. Section 2 describes the measurements and data. Section 3 describes the new methodology in terms of the definition and implementation. The performance of the method is demonstrated in Section 4, and a summary is presented in Section 5.

2 Data Descriptions

2.1 Radiosonde

RS launches took place at least four times per day at the ARM SGP site, usually at 0030, 0630, 1230, and 1830 local time (LT). Holdridge et al. (2011) provide technical details about the ARM RS (https://www.arm.gov/capabilities/instruments/sonde). In this study, we consistently use daylight saving time (Coordinated Universal Time -5 h) as local time throughout the year to avoid inconsistencies between summer and winter. Besides the routine

https://doi.org/10.5194/acp-2021-302
Preprint. Discussion started: 1 July 2021


Atmospheric Chemistry and Physics Discussions

measurements, there are fewer, but still considerable numbers of RS data obtained at other times of the day (e.g., 0930, 1200, 1300, 1530, and 1900 LT). These supplemental RS samples at other times comprise ~10% of the total number of cases. RS data from 0630–1900 LT are utilized in this study. The vertical resolution of RS data varies according to the rising rate of the balloon, but measurements are generally taken ~10 m apart. We further vertically average the RS data to achieve a vertical resolution of 5 hPa. By using the well-established method developed by Liu and Liang (2010), we retrieved PBLHs over the SGP site from RS measurements. The potential temperature is corrected as the virtual potential temperature, θ_v, using the water vapor mixing ratio [WVMR; $\theta_v = (1 + 0.61\mathrm{WVMR})$]. The virtual potential temperature does not include a correction for the liquid water content profile, as this is challenging to measure in many conditions. Therefore, the virtual potential temperature is not conserved during moist convection. Since we mainly focus on the sub-cloud atmosphere, this is not a serious problem. Moreover, we use scaled RS moisture profiles normalized by the total precipitable water vapor derived from the microwave radiometer (https://www.arm.gov/capabilities/vaps/lssonde, Revercomb et al., 2003).

2.2 Micropulse lidar (MPL) system

MPL backscatter profiles were collected at the SGP site from September 1998 to July 2019 with high continuity (Campbell et al., 2002). Technical details and data availability can be found at the website

https://doi.org/10.5194/acp-2021-302
Preprint. Discussion started: 1 July 2021


Atmospheric Chemistry and Physics Discussions

https://www.arm.gov/capabilities/instruments/mpl. The backscatter profiles have a vertical resolution of 30 m. MPL signals have an initial temporal resolution of 10–30 s and are averaged every 10 min for this study. Due to the inherent problem of lidar observations, there is a ~0.2-km near-surface "blind zone". Following the standard lidar-data processing, background subtraction, signal saturation and overlapping, after-pulse and range corrections are applied to the raw MPL data (Campbell et al., 2002, 2003). Questionable data are excluded based on the quality-control flags.

2.3 Cloud product

The MPL can be used to detect cloud layers based on signal gradients (Platt et al., 1994). Lidar-based methods are accurate for determining the cloud-base height (CBH) but may miss information about the cloud top due to the signal saturation within an optically thick cloud (Clothiaux et al., 2000). Under this condition, the cloud radar provides a better estimation of the cloud-top height (CTH). In this study, we directly use an existing quality-controlled cloud product, CLDTYPE/ARSCL (https://www.arm.gov/capabilities/vaps/cldtype), which combines information from the MPL, ceilometer, and cloud radar to determine the vertical boundaries of clouds (Clothiaux et al., 2000; Flynn et al., 2017). For the lowest cloud base, the best estimation from laser-based techniques (i.e., MPL and ceilometer) is used. The original temporal resolution of the CLDTYPE/ARSCL product is 1 min, averaged to a 10-min temporal resolution. To avoid averaging jumps in signal between different

https://doi.org/10.5194/acp-2021-302
Preprint. Discussion started: 1 July 2021


Atmospheric Chemistry and Physics Discussions

clouds, a cloud is considered to be continuous if its base height varies less than 0.25 km between two consecutive profiles.

3 Methodology

3.1 Definition of coupled and decoupled clouds based on thermodynamics

The definition of the state of cloud-surface coupling over land is a critical question. For marine stratocumulus, coupled clouds are identified when the liquid water potential temperature varies less than a certain threshold (i.e., 0.5 K) below the cloud base (Jones et al., 2011). We try to extend the concept of coupling and decoupling to clouds over land. The PBL over land is typically buoyancy driven and controlled by surface fluxes during the daytime. We consider a cloud is in the coupled state when it strongly interacts with the buoyancy fluxes within the PBL.

Figure 1 presents the idealized vertical profiles of virtual potential temperature (θ_v) under the clear-sky, coupled cloud, and decoupled cloud. A superadiabatic surface layer exchanges the heat fluxes between the surface and PBL. The outer layer and entrainment zone are turbulently coupled with the surface, and thus, are considered as the coupled regime. Meanwhile, the free atmosphere is considered as the decoupled regime. Theoretically, θ_v is constant in the outer layer, and follows the wet adiabatic lapse rate in the cloud layer. Although the profiles of θ_v in the real atmosphere can largely differ from the idealized profiles, the relative position between the cloud layer and capping inversion of entrainment zone is clear. For the coupled cases, the cloud

https://doi.org/10.5194/acp-2021-302
Preprint. Discussion started: 1 July 2021


Atmospheric Chemistry and Physics Discussions

base is below the capping inversion of entrainment zone. For the decoupled cases, the cloud base is above the capping inversion. Based on this feature, we can use the virtual potential temperature profiles to diagnose the coupling state of low clouds.

We first look at several examples of profiles of θ_v and WVMR from the RS (Figure 2). If the CBH is lower than the PBLH, the cloud is affected by turbulence and buoyancy fluxes in the PBL, such as the cases shown in Figure 2a. Note that the PBLH is not an absolute boundary limiting turbulence and buoyancy fluxes. Due to the overshooting of rising air parcels, we use a range to screen the condition of coupled clouds. As shown in Figure 2b, even when the CBH is slightly above the PBLH, WVMR and θ_v are still relatively consistent between the cloud layer and the PBL and show large step signals at the cloud top.

Figure 2c-d shows a clear inversion layer between the cloud base and the PBL top, and the difference in θ_v between the CBH and the PBLH ($\Delta\theta_v$) is relatively large. Such a notable inversion layer prevents the buoyancy fluxes within the PBL from reaching the cloud base, leading to the decoupling between the cloud and the PBL. Overall, whether there is a clear inversion between the cloud base and the PBL top is the key factor in determining coupling and decoupling. In this aspect, $\Delta\theta_v$ is the key factor. In Figure 2, $\Delta\theta_v$ for coupled cases (a-c) is -0.32 K and 0.31 K, respectively, and $\Delta\theta_v$ for decoupled cases (d-e) is 1.47 K and 5.0 K, respectively.

Therefore, instead of giving a height range to limit the differences between CBH and PBLH, we consider using the differences in θ_v between CBH and PBLH ($\Delta\theta_v = \theta_v^{CBH} - \theta_v^{PBLH}$) to determine the threshold for distinguishing coupled and decoupled

https://doi.org/10.5194/acp-2021-302
Preprint. Discussion started: 1 July 2021


Atmospheric Chemistry and Physics Discussions

clouds. For decoupled cases, the cloud base is above the capping inversion of entrainment zone. There is a notable inversion in θ_v between PBL top and decoupled cloud base. Thus, we identify the cases satisfying $\Delta\theta_v > \delta_s$ as being in a decoupled state. Correspondingly, we identify the cases satisfying $\Delta\theta_v < \delta_s$ as being in a coupled state. We set the range of CBH to between 0 and 4 km and excluded cases of deep convection (i.e., CBH < 4 km and CTH > 6.5 km).

For identical cases, θ_v is constant within the PBL. Under this assumption, δ_s can be set as 0. However, there are certain variations in θ_v within the PBL, which can cause inversions with relatively small magnitudes between the cloud base and PBL top. Figure 3a presents the inversion strength in θ_v within PBL during the daytime. The inversions near surface or across the PBL top are excluded. Besides the capping inversion and surface inversion, the inversion strength within PBL is typically below 1K. Therefore, we set δ_s as 1 K, which is the same as the criterion for determining stable or convective conditions (Liu & Liang, 2010). Furthermore, we demonstrate the probability density function (PDF) of $\Delta\theta_v$ for the low cloud cases. Coupled and decoupled clouds are classified by the threshold of δ_s (1 K). Through the development of PBL, boundary layer clouds frequently occur in the entrainment zone, and form a coupled cloud-PBL system. For such coupled systems, θ_v at cloud top and PBL top is highly consistent for the majority of cases. Thus, the PDF of $\Delta\theta_v$ shows significantly high values for the range of -2 K to 0.5 K in the coupled regime. Meanwhile, the PDF of $\Delta\theta_v$ is evenly distributed in the decoupled regime. Since we only analyze low clouds, the PDF of $\Delta\theta_v$ slowly decrease when $\Delta\theta_v$ is above 10 K.

https://doi.org/10.5194/acp-2021-302
Preprint. Discussion started: 1 July 2021


Atmospheric Chemistry and Physics Discussions

Based on the variations in θ_v within PBL, we set δ_s as 1 K. However, it should note that it is not an absolute value. A similar threshold of 0.5 K has been used for marine stratocumulus (Jones et al., 2011; Dong et al., 2015). Comparing to the marine condition, θ_v show greater variabilities over land. Hence, the threshold is correspondingly larger. On the other hand, since the threshold of 1 K is in the low PDF regime (Figure 3b), the small changes in this value would not notably affect the identifications. Specifically, a 0.1 K difference in δ_s will lead to a 0.5% difference in the identification of coupled cloud.

Following the traditional definition of buoyancy forces (Wallace & Hobbs, 2006), we further integrate the buoyancy forces within the lowest 1 km ($-g\int_0^{1km}\frac{1}{\theta}\frac{\Delta\theta}{\Delta z}dz$). Figure 4 shows the relationships between CBH and buoyancy forces in the lower atmosphere for $\Delta\theta_v < \delta_s$ (coupled state) and $\Delta\theta_v > \delta_s$ (decoupled state). In terms of the responses to buoyancy forces, dramatic differences between coupled and decoupled clouds are seen. Following our previous study (Su et al., 2018), we use the inverse fitting ($f(x) = A/x + B$) with consideration of density to establish the relationship between CBH and buoyancy forces. The magnitude of the correlation coefficient ($R^{\dagger}$) is designed to measure the degree to which the data fit an inverse relationship. For a coupled cloud, changes in CBH to variable buoyancy forces mostly follow an inverse function. For the coupled cases, strong buoyancy forces are associated with a thick PBL and high CBH. Since a decoupled cloud occurs in the free atmosphere, the CBH of a decoupled cloud has a very weak linkage with the buoyancy forces.

https://doi.org/10.5194/acp-2021-302
Preprint. Discussion started: 1 July 2021


Atmospheric Chemistry and Physics Discussions

232

233 *3.2 Lidar-based method to identify coupled and decoupled clouds*

234 *3.2.1 Method description*

235 Given the rapid change in clouds over land, RS observations have limitations
236 when it comes to tracking cloud development due to the coarse temporal resolution
237 and drifting of the balloon. We thus further developed a lidar-based method to identify
238 the coupled states of clouds based on our new algorithm for retrieving the PBLH that
239 can better track the diurnal variations in PBLH than conventional lidar-based
240 approaches (Su et al., 2020). We adapted this algorithm for retrieving the PBLH and
241 developed a new scheme to deal with cloudy conditions. The principles behind the
242 PBLH algorithm are stated next for completeness.

243 Our new PBLH algorithm can retrieve the PBL variability from the MPL under
244 Different Thermo-Dynamic Stability (thus named the DTDS algorithm) conditions,
245 taking into account the vertical coherence and temporal continuity of the PBLH. First,
246 we identify the local maximum positions (LMPs; range: 0.25–4 km) in profiles of the
247 wavelet covariance transform function derived from lidar backscatter (Brooks, 2003).
248 These LMPs are the potential positions of the PBLH. We can use the PBLH derived
249 from morning RS soundings as the starting point. Without morning RS soundings, the
250 algorithm can still work well, with the lowest LMPs selected as the starting point,
251 which reduces by 0.02–0.05 the correlation coefficient between MPL-derived and
252 RS-derived PBLHs (Su et al., 2020).

https://doi.org/10.5194/acp-2021-302
Preprint. Discussion started: 1 July 2021


Atmospheric Chemistry and Physics Discussions

253 To ensure good continuity, we select the closest LMP to the earlier position of the
254 PBLH. Different stages of PBL development are considered. DTDS-derived PBLHs
255 likely increase during the growth stage and decrease during the decaying stage, but
256 the algorithm is also able to identify decreases during the growth stage or increases
257 during the decaying stage based on the selection scheme described by Su et al. (2020).
258 There are multiple step signals in the backscatter profiles when complex aerosol
259 structures (e.g., the residual layer) are present, leading to multiple LMPs. Based on
260 temporal continuity, we select the appropriate LMP as the position of the PBL top.
261 However, PBLH retrievals still suffer from relatively low accuracies under stable
262 conditions because of the weak vertical mixing and residual layer.

263 Clouds induce strong step signals in the lidar backscatter, further considerably
264 affecting PBLH retrievals. Su et al. (2020) only considered cases where the low cloud
265 top coincided with the previous PBL top, excluding other low-cloud cases (> 60% of
266 all low-cloud cases). Here, we specifically consider coupled and decoupled states of
267 low clouds. Due to the MPL's ~0.2-km blind zone, we only analyze the PBLH and
268 CBH above 0.2 km. Figure 5 presents the flow chart describing the updated DTDS
269 algorithm. In particular, we jointly use PBL development and the LCL to diagnose the
270 states of coupling or decoupling. In ideal situations, LCL, PBLH, and CBH are highly
271 consistent with each other for coupled clouds. But for real conditions, we only require
272 that either the LCL or the PBLH coincides with the CBH for identifying coupled cases,
273 with another parameter serving as an additional constraint. Specifically, a coupled
274 cloud needs to occur within a certain range of LCL and the previous position of the

https://doi.org/10.5194/acp-2021-302
Preprint. Discussion started: 1 July 2021


Atmospheric Chemistry and Physics Discussions

PBL top. For the DTDS algorithm, five empirical parameters are used, including A_1, A_2, A_3, A_4, A_5. As listed in the Table 1, $A_1 - A_5$ are set as 0.7, 0.2, 0.15, 1.35, and 1.1, respectively. A cloud at time i is identified as being in the coupled state if the CBH is less than $[H(i-1) + 0.2 \text{ km } (A_2)]$ and [LCL+ 0.7 km (A_1)]. A cloud is also considered to be in a coupled state if the CBH is coincident with the LCL within 0.15 km (A_3), and the CBH is less than $[H(i-1) + 0.7 \text{ km } (A_1)]$, where $H(i-1)$ represents the PBLH at time $(i-1)$. The LCL is calculated from surface meteorological data (relative humidity, temperature, pressure) at the SGP site based on an exact expression (Romps, 2017).

After determining the coupling or decoupling state of a cloud, we retrieve $H(i)$ (i.e., PBLH at time *i*) based on the cloud state. For decoupled cases, we use the same strategy for a clear sky to retrieve the PBLH. Based on the selection scheme in the DTDS algorithm, the LMP below the CBH is selected as $H(i)$. For coupled cases, we jointly use CBH and CTH to determine PBLH. During the warm season, shallow cumulus often occurs in the upper part of the PBL with strong surface heating, so the CTH can be regarded as the PBLH (Stull, 1988; Wallace & Hobbs, 2006). Under this condition, the CTH coincides with the previous PBL top. Therefore, if [CTH $<$ $PBLH_{30min} + 0.2\ km\ (A_2)$], we set $H(i)$ equal to the minimum between CTH and the product A_4*CBH, where $PBLH_{30min}$ is the average value of the PBLH within 30 min of the prior time *i*. Since this does not work for the active cloud (i.e. a cloud that reaches its level of free convection), we set $H(i) = A_5$CBH, if [CTH $\geqslant$ $PBLH_{30min} +$ $0.2\ km\ (A_2)$]. After retrieving $H(i)$, we consider that the cloud above the PBLH is

https://doi.org/10.5194/acp-2021-302
Preprint. Discussion started: 1 July 2021


Atmospheric Chemistry and Physics Discussions

still coupled if $[\mathrm{CBH} < H(i) + 0.2\ km\ (A_2)]$. Moreover, we added an upper limit for all PBLH retrievals. If $[H(i) > \mathrm{LCL} + 0.7\ km\ (A_1)]$, we adjust $H(i)$ as the maximum LMP below the LCL. The new DTDS method combines lidar measurements and surface meteorological observations and can simultaneously retrieve the PBLH and cloud states.

3.2.2 Selection of empirical parameters

The states of coupling and decoupling are diagnostic parameters rather than explicit expressions. Similar to the other methods for retrieving PBLH (e.g., Brooks, 2003; Liu & Liang, 2010), multiple empirical parameters are used to determine PBLH. Here we discuss the selection of empirical parameters in the algorithm.

Note that we used the CTH and A_4*CBH as the upper limits for PBLH retrievals in the DTDS algorithm. For coupled cases, these two limits are generally close to or above the position of the PBL top. Only 2% (3%) of total cases meet the condition that the RS-derived PBLH is 0.25 km higher than the CTH (A_4*CBH). Section 4 presents the detailed relationships between CBH, CTH, and PBLH. In the DTDS method, CTH serves as the upper limit for PBLH under the condition of coupled shallow cumulus.

Similar to previous studies, we can also use the LCL as the standard to identify coupled clouds (Dong et al., 2015; Zheng & Rosenfeld, 2015). We assume a cloud is coupled if $|\mathrm{CBH} - \mathrm{LCL}| <$ some criteria. Figure 6a shows the commission errors and

https://doi.org/10.5194/acp-2021-302
Preprint. Discussion started: 1 July 2021


Atmospheric Chemistry and Physics Discussions

318 omission errors for different criteria. Here, the commission error is calculated as the
319 percentage of decoupled clouds misidentified as coupled clouds. The commission
320 error can also be called a "false positive", as the former is a common term for
321 describing the nature of an error in identification. The omission error is calculated as
322 the percentage of coupled clouds that have not been identified under this criterion. By
323 using the LCL, we can obtain a relatively low commission error if the criterion is less
324 than 0.15 km and a relatively low omission error if the criterion is greater than 0.7 km.
325 Thus, we set A_1 and A_3 as 0.7 and 0.15 in the DTDS method to exclude and to
326 select cases of coupled clouds. We can also use the RS-derived PBLH as the criterion
327 (Figure 6b). Despite the coarse temporal resolution, the RS-derived PBLH can be a
328 good criterion to use to distinguish between coupling and decoupling. If we consider a
329 coupled cloud as a cloud where (CBH < RS-derived PBLH + 0.2 km), both
330 commission and omission errors are ~5%. Therefore, we primarily use [PBLH+0.2
331 km (A_2)] in the DTDS method to identify coupled and decoupled regimes.

332 Moreover, we test the sensitivity of selecting these empirical parameters. Figure 7
333 presents the commission errors and omission errors in the identifications of coupled
334 clouds for selecting different values of empirical parameters. Among these parameters,
335 A_2 is the critical one, which would notably affect the identification results. In general,
336 A_2 determine the maximum differences between PBLH and CBH for coupled cases.
337 If [CBH-PBLH > A_2], we consider the cloud is under the decoupled state. Thus, the
338 identification method is quite sensitive to A_2. Selecting a low value of A_2 would
339 neglect many coupled cases, which leads to a high omission error. Meanwhile,

https://doi.org/10.5194/acp-2021-302
Preprint. Discussion started: 1 July 2021


Atmospheric Chemistry and Physics Discussions

selecting a high value of A_2 would misclassify many coupled cases, which leads to a high commission error. After a trail and error, A_2 is set as 0.2 km to balance the omission and commission errors. The selections for other parameters are not sensitive for the coupled cloud identifications. We can choose them from a reasonable range.

As a by-product of this method, we also pay attentions to the PBLH retrievals under cloudy conditions. Figure 8 presents the mean absolute biases and correlation coefficients between PBLH derived from lidar and radiosonde for selecting different values of empirical parameters. To match the scope of this study, we only analyze the low cloud conditions. For retrieving PBLH under cloudy conditions, A_2 is the critical parameter. The variations in correlation coefficients under different values of empirical parameters are small with a range of 0.81-0.82. However, the absolute biases can considerably differ under different values of A_5. In general, A_5 represents the ratio between CBH and PBLH under coupled conditions. If A_5 is above 1.1, PBLH retrievals under cloudy conditions are overestimated. We set A_5 as 1.1 to achieve a relatively low biases and a relatively high correlation coefficient at the same time. For other parameters, the selections from reasonable ranges would not notably affect the PBLH retrievals.

In short, selections of these empirical parameters are based on the overall relationship between cloud and PBL under the coupled and decoupled states. In our method, the selection of A_2 is critical for the identifications of coupled clouds, while the selection of A_5 is critical for the PBLH retrievals under cloudy conditions. The selections of other parameters are not sensitive.

https://doi.org/10.5194/acp-2021-302
Preprint. Discussion started: 1 July 2021


Atmospheric Chemistry and Physics Discussions

362

363 **4 Results**

364 Figure 9 illustrates four examples of PBLH retrievals and cloud states derived
365 from the DTDS algorithm for 27 October 2011, 31 July 2002, 19 March 2000, and 1
366 May 2012. Figure 9a depicts coupled shallow cumulus occurring at noontime at the
367 PBL top. With a weak surface flux of ~200 W m^{-2}, this shallow cumulus cloud
368 appeared for less than an hour. Figure 9b shows a developed coupled cumulus cloud.
369 With a strong surface flux of ~500 W m^{-2}, this coupled cloud continuously developed
370 during the daytime. Figure 9c presents the case of a daylong coupled cloud. After the
371 passage of a frontal system that day, stratocumulus occurred during the morning with
372 a cloud thickness of 0.5 km. Through the development of the PBL, the thick
373 stratocumulus cloud was broken up by the strong turbulences, transforming into
374 shallow cumulus clouds. Figure 9d shows the case of an active coupled cloud, which
375 is generally associated with a large amount of convective available potential energy.
376 Even though coupled clouds can differ in appearance and variability throughout the
377 day, the common feature is the coherent variation between the cloud base and the PBL
378 top. The LCL is a relevant parameter and can differ from the PBLH and the CBH for
379 some coupled cases (e.g., Figure 9b-c).

380 The identification accuracy, or disparity between different methods, are evaluated
381 in terms of the selected criteria, for which the identification method based on $\Delta\theta_v$ is
382 regarded as the "truth", as described in Section 3.1. Hereafter, all results are analyzed
383 for the period of 1000–1900 LT, so early-morning data are not used. The commission

https://doi.org/10.5194/acp-2021-302
Preprint. Discussion started: 1 July 2021


Atmospheric Chemistry and Physics Discussions

error is 10.1%, and the omission error is 6.8% for the DTDS method. Note that lidar-based PBLH methods generally suffer from relatively low accuracy under stable atmospheric conditions. Following Liu and Liang (2010), we identified stable PBLs from RS measurements. Since coupled clouds are driven by relatively strong buoyancy fluxes, only 1% of total cases of coupled clouds occurred under stable PBL conditions during the study period (0700–1900 LT). Therefore, the relatively low accuracy for stable PBLs is not a major problem in this study.

Figure 6 also compares the accuracy between the DTDS and LCL methods. Based on the LCL alone, we cannot choose an appropriate criterion to achieve a lower commission error and omission error simultaneously. Thus, we do not use the LCL as the single standard to detect the coupling and decoupling of low clouds in our study. As diagnostic parameters, different methods inevitably produce different results regarding coupling and decoupling. Although we consider the method based on $\Delta\theta_v$ as the standard, it still suffers from uncertainties arising from balloon drifting. From this perspective, it is hard to conclude which method is the best. Since it determines the PBLH based on aerosol backscattering, the lidar-based method may be more representative of the coupling between a cloud and the aerosol layer near the surface when clear skies occur, at least during a short window of time.

Figure 10a-b presents the occurrence frequencies of the CBH and the CTH at different heights. Despite the same variation ranges, clouds are mostly coupled if the CBH is lower than 1 km, while decoupled clouds dominate if the CBH is higher than 3 km. Figure 10c-d shows the changes in the coupled fraction (ratio of coupled cases

https://doi.org/10.5194/acp-2021-302
Preprint. Discussion started: 1 July 2021


Atmospheric Chemistry and Physics Discussions

406 to total cases) with different CBHs and CTHs. The coupled fraction is about 90% if
407 the CBH is lower than 1 km and decreases to 2% for CBHs above 3 km. Although the
408 CBHs for coupled cases are generally less than 3 km, CTHs for coupled cases can be
409 much higher. Coupled clouds still account for around 10% of the cases with CTHs
410 above 6 km.

411 Figure 11 shows scatter plots between CBH, CTH, PBLH, and LCL for coupled
412 and decoupled clouds. For coupled clouds, there is a generally strong correlation
413 between CBH, LCL, and PBLH, contrary to the weak relationships of decoupled cases.
414 The relationship between CTH and RS-derived PBLH is complicated. For shallow
415 cumulus clouds, their tops can be considered as PBL tops for the coupled state, while
416 the cloud top is considerably above the position of the PBL top for active cumulus
417 clouds. We also note that the accuracy of CTH retrievals is generally lower than the
418 accuracy of CBH retrievals (Clothiaux et al., 2000). As CTH is not a criterion for
419 cloud coupling, the accuracy of CTH would not affect the identification of coupled
420 cloud, but may affect the PBLH retrievals for the coupled cloud cases.

421 For coupled clouds, the DTDS-derived PBLH relies on the cloud position,
422 showing a strong correlation with the RS-derived PBLH with a correlation coefficient
423 (R) of ~0.9 (Figure 11d), since the position of the coupled cloud serves as a good
424 reference for determining the PBLH. For decoupled cases, the correlation between the
425 DTDS-derived PBLH and the RS-derived PBLH is generally good (R = 0.73) but
426 worse than the correlation for coupled cases. As pointed out in previous studies (Chu
427 et al., 2019; Hageli et al., 2000; Lewis et al., 2013; Su et al., 2017b), it has been a

https://doi.org/10.5194/acp-2021-302
Preprint. Discussion started: 1 July 2021


Atmospheric Chemistry and Physics Discussions

persistent problem to retrieve the PBLH under cloudy conditions since the large backscatter and step signals from cloud interference would be excluded to avoid interfering with the retrievals. After identifying the coupling or decoupling of clouds, the PBLH can be successfully retrieved under cloudy conditions.

Compared to the clear-sky cases discussed in previous studies (e.g., Chu et al., 2019; Yang et al., 2017), the DTDS-derived PBLH shows a much higher correlation with RS-derived PBLH for coupled cloud cases and has a similar R as the RS-derived PBLH for decoupled cloud cases. Moreover, due to the different definitions of the PBLH and aerosol stratification within the PBL, there are always considerable differences between lidar- and RS-derived PBLHs, which cannot be eliminated by a specific algorithm (Chu et al., 2019; Su et al., 2020).

5 Summary

In this study, we proposed a novel method for distinguishing between coupled and decoupled low clouds over land. Based on the understanding of PBL processes and quantitative analyses, we developed a lidar-based method (DTDS) to identify the coupling state of low clouds over the SGP site. In practice, we identified a coupled cloud when the position of the cloud base was generally close to or lower than the previous position of the PBL top, with the LCL serving as an additional restriction. Compared to using the LCL alone, the coupled states identified by the DTDS method show better consistency with the results derived from radiosondes, with about 10% differences between the lidar-based retrievals and radiosonde results.

https://doi.org/10.5194/acp-2021-302
Preprint. Discussion started: 1 July 2021


Atmospheric Chemistry and Physics Discussions

Not only coupled state, the method also can provide high-quality retrievals of the PBLH under cloudy conditions. A long-lasting problem with lidar-retrieval of PBLH is either incapability of retrieval or large uncertainties induced by the occurrence of low clouds (e.g., Chu et al., 2019; Hageli et al., 2000; Lewis et al., 2013), we address this issue by separately considering the coupled and decoupled of low clouds. Specifically, in coupled conditions, the position of the coupled cloud serves as a good reference for identifying the PBLH. In decoupled conditions, the large backscatter and step signals from clouds would be excluded to avoid interfering with the retrievals. With our method, cloudy conditions are well handled.

With the new method, we study the difference of cloud-PBL interactions in coupled and decoupled conditions. In contrast to the sensitive responses of coupled clouds to changes in the PBLH and buoyancy, the decoupled clouds and the PBLH are weakly related. Due to their different relationships with the PBL, a robust distinguishment between the coupled and decoupled low clouds is critical for further investigating the coupled land-atmosphere system and aerosol-cloud interactions. Our methodology paves a solid ground for such pursuits.

Code/Data availability. All these datasets are publicly available at the ARM archive https://adc.arm.gov/discovery/#/results/site_code::sgp. The products developed in this study, i.e., cloud states and the PBLH, are currently available upon request from the lead author (tianning@umd.edu) and are expected to be added to the ARM archive in the near future. The code of this method is available upon request from the lead author

https://doi.org/10.5194/acp-2021-302
Preprint. Discussion started: 1 July 2021


Atmospheric Chemistry and Physics Discussions

(tianning@umd.edu).

Author contribution. T.S. and Z.L. conceptualized this study. T.S. carried out the analysis, with comments from other co-authors. T.S., Y.Z., and Z.L. interpreted the data and wrote the manuscript.

Competing interests. The authors declare that they have no conflict of interest.

Acknowledgements. This work was supported by grants from the U.S. Department of Energy (DE-SC0018996), the National Science Foundation (AGS1837811), and NASA (NNX16AN61G). We acknowledge the provision of radiosonde, MPL data, surface meteorological data, and cloud products by the U.S. Department of Energy's ARM program.

References

Betts, A.K. (2009). Land-surface-atmosphere coupling in observations and models. *Journal of Advances in Modeling Earth Systems*, *1*(3). https://doi.org/10.3894/JAMES.2009.1.4

Revercomb, H.E., Turner, D.D., Tobin, D.C., Knuteson, R.O., Feltz, W.F., Barnard, J.,

https://doi.org/10.5194/acp-2021-302
Preprint. Discussion started: 1 July 2021


Atmospheric Chemistry and Physics Discussions

491 Bösenberg, J., Clough, S., Cook, D., Ferrare, R. and Goldsmith, J., 2003. The
492 ARM program's water vapor intensive observation periods: Overview, initial
493 accomplishments, and future challenges. Bulletin of the American Meteorological
494 Society, 84(2), pp.217-236.

495 Bretherton, C. S., & Wyant, M. C. (1997). Moisture transport, lower-tropospheric
496 stability, and decoupling of cloud-topped boundary layers. *Journal of the*
497 *Atmospheric Sciences*, *54*(1), 148–167.
498 https://doi.org/10.1175/1520-0469(1997)054<0148:MTLTSA>2.0.CO;2

499 Brooks, I. M. (2003). Finding boundary layer top: application of a wavelet covariance
500 transform to lidar backscatter profiles. *Journal of Atmospheric and Oceanic*
501 *Technology*, *20*, 1092–1105.
502 https://doi.org/10.1175/1520-0426(2003)020<1092:FBLTAO>2.0.CO;2

503 Campbell, J.R., Welton, E.J., Spinhirne, J.D., Ji, Q., Tsay, S.C., Piketh, S.J.,
504 Barenbrug, M. and Holben, B.N., 2003. Micropulse lidar observations of
505 tropospheric aerosols over northeastern South Africa during the ARREX and
506 SAFARI 2000 dry season experiments. Journal of Geophysical Research:
507 Atmospheres, 108(D13).

508 Campbell, J. R., Hlavka, D. L., Welton, E. J., Flynn, C. J., Turner, D. D., Spinhirne, J.
509 D., … Hwang, I. H. (2002). Full-time, eye-safe cloud and aerosol lidar
510 observation at atmospheric radiation measurement program sites: instruments and
511 data processing. *Journal of Atmospheric and Oceanic Technology*, *19*(4), 431–442.

https://doi.org/10.1175/1520-0426(2002)019<0431:FTESCA>2.0.CO;2

Cheruy, F., Dufresne, J. L., Hourdin, F., & Ducharne, A. (2014). Role of clouds and land-atmosphere coupling in midlatitude continental summer warm biases and climate change amplification in CMIP5 simulations. *Geophysical Research Letters*, *41*(18), 6493–6500. https://doi.org/10.1002/2014GL061145

Chu, Y., Li, J., Li, C., Tan, W., Su, T., & Li, J. (2019). Seasonal and diurnal variability of planetary boundary layer height in Beijing: intercomparison between MPL and WRF results. *Atmospheric Research*, *227*, 1–13. https://doi.org/10.1016/j.atmosres.2019.04.017

Clothiaux, E. E., Ackerman, T. P., Mace, G. G., Moran, K. P., Marchand, R. T., Miller, M. A., & Martner, B. E. (2000). Objective determination of cloud heights and radar reflectivities using a combination of active remote sensors at the ARM CART sites. *Journal of Applied Meteorology*, *39*(5), 645–665. https://doi.org/10.1175/1520-0450(2000)039<0645:ODOCHA>2.0.CO;2

Demoz, B., Flamant, C., Weckwerth, T., Whiteman, D., Evans, K., Fabry, F., …. & Schwemmer, G. (2006). The dryline on 22 May 2002 during IHOP_2002: convective-scale measurements at the profiling site. *Monthly Weather Review*, *134*(1), 294–310. https://doi.org/10.1175/MWR3054.1

Dong, X., Schwantes, A. C., Xi, B., & Wu, P. (2015). Investigation of the marine boundary layer cloud and CCN properties under coupled and decoupled conditions over the Azores. *Journal of Geophysical Research: Atmospheres*, *120*,

https://doi.org/10.5194/acp-2021-302
Preprint. Discussion started: 1 July 2021

6179–6191. https://doi.org/10.1002/2014JD022939

Driedonks, A. G. M. (1982). Models and observations of the growth of the atmospheric boundary layer. *Boundary-Layer Meteorology*, *23*(3), 283–306. https://doi.org/10.1007/BF00121117

Ek, M. B., & Holtslag, A. A. M. (2004). Influence of soil moisture on boundary layer cloud development. *Journal of Hydrometeorology*, *5*(1), 86–99. https://doi.org/10.1175/1525-7541(2004)005<0086:IOSMOB>2.0.CO;2

Flynn, D., Shi, Y., Lim, K., & Riihimaki, L. (2017). Cloud Type Classification (cldtype) Value-Added Product. Ed. by Robert Stafford, ARM Research Facility. DOE/SC-ARM-TR-200.

Garratt, J. R. (1994). Review: the atmospheric boundary layer. *Earth-Science Reviews*, *37*(1-2), 89–134. https://doi.org/10.1016/0012-8252(94)90026-4

Glenn, I. B., Feingold, G., Gristey, J. J., & Yamaguchi, T. (2020). Quantification of the radiative effect of aerosol-cloud-interactions in shallow continental cumulus clouds. *Journal of the Atmospheric Sciences*, *77*, 2905–2920. https://doi.org/10.1175/JAS-D-19-0269.1

Golaz, J. C., Larson, V. E., & Cotton, W. R. (2002). A PDF-based model for boundary layer clouds. Part I: Method and model description. *Journal of the Atmospheric Sciences*, *59*(24), 3540–3551. https://doi.org/10.1175/1520-0469(2002)059<3540:APBMFB>2.0.CO;2

https://doi.org/10.5194/acp-2021-302
Preprint. Discussion started: 1 July 2021


Atmospheric Chemistry and Physics Discussions

553 Guo, J., Miao, Y., Zhang, Y., Liu, H., Li, Z., Zhang, W., … Zhai, P. (2016). The
554 climatology of planetary boundary layer height in China derived from radiosonde
555 and reanalysis data. *Atmospheric Chemistry and Physics*, *16*(20), 13,309–13,319.
556 https://doi.org/10.5194/acp-16-13309-2016

557 Hageli, P., Steyn, D. G., & Strawbridge, K. B. (2000). Spatial and temporal variability
558 of mixed-layer depth and entrainment zone thickness. *Boundary-Layer*
559 *Meteorology, 97*, 47–71. https://doi.org/10.1023/A:1002790424133

560 Holdridge, D., Ritsche, M., Prell, J., & Coulter, R. (2011). Balloon-borne sounding
561 system (SONDE) handbook. https://www.arm.gov/capabilities/instruments/sonde

562 Jones, C., Bretherton, C., & Leon, D. (2011). Coupled vs. decoupled boundary layers
563 in VOCALS-REx. *Atmospheric Chemistry and Physics*, *11*(14), 7143–7153.
564 https://doi.org/10.5194/acp-11-7143-2011

565 Kasahara, A. (1974). Various vertical coordinate systems used for numerical weather
566 prediction. *Monthly Weather Review*, *102*(7), 509–522.
567 https://doi.org/10.1175/1520-0493(1974)102<0509:VVCSUF>2.0.CO;2

568 Lewis, J. R., Welton, E. J., Molod, A. M., & Joseph, E. (2013). Improved boundary
569 layer depth retrievals from MPLNET. *Journal of Geophysical Research:*
570 *Atmospheres*, *118*(17), 9870–9879. https://doi.org/10.1002/jgrd.50570

571 Liu, S. Y., & Liang, X. Z. (2010). Observed diurnal cycle climatology of planetary
572 boundary layer height. *Journal of Climate*, *23*, 5790–5809.
573 https://doi.org/10.1175/2010JCLI3552.1

https://doi.org/10.5194/acp-2021-302
Preprint. Discussion started: 1 July 2021


Atmospheric Chemistry and Physics Discussions

574 Nicholls, S. (1984). The dynamics of stratocumulus: aircraft observations and
575 comparisons with a mixed layer model. *Quarterly Journal of the Royal*
576 *Meteorological Society*, *110*(466), 783–820.
577 https://doi.org/10.1002/qj.49711046603

578 Platt, C. M., Young, S. A., Carswell, A. I., Pal, S. R., McCormick, M. P., Winker, D.
579 M., … & Wooldridge, C. (1994). The Experimental Cloud LIdar Pilot Study
580 (ECLIPS) for cloud-radiation research. *Bulletin of the American Meteorological*
581 *Society*, *75*, 1635–1654.
582 https://doi.org/10.1175/1520-0477(1994)075<1635:TECLPS>2.0.CO;2

583 Romps, D. M. (2017). Exact expression for the lifting condensation level. *Journal of*
584 *the Atmospheric Sciences*, *74*(12), 3891–3900.
585 https://doi.org/10.1175/JAS-D-17-0102.1

586 Santanello Jr., J. A., Dirmeyer, P. A., Ferguson, C. R., Findell, K. L., Tawfik, A. B.,
587 Berg, A., … & Roundy, J. (2018). Land–atmosphere interactions: the LoCo
588 perspective. *Bulletin of the American Meteorological Society*, *99*(6), 1253–1272.
589 https://doi.org/10.1175/BAMS-D-17-0001.1

590 Sawyer, V., & Li, Z. Q. (2013). Detection, variations and intercomparison of the
591 planetary boundary layer depth from radiosonde, lidar and infrared spectrometer.
592 *Atmospheric Environment*, *79*, 518–528.
593 https://doi.org/10.1016/j.atmosenv.2013.07.019

594 Stull, R. B. (1988). *An Introduction to Boundary Layer Meteorology*. Dordrecht:

https://doi.org/10.5194/acp-2021-302
Preprint. Discussion started: 1 July 2021

Atmospheric Chemistry and Physics Discussions

595 Springer Netherlands.

596 Su, T., Li, J., Li, J., Li, C., Chu, Y., Zhao, Y., … Wang, L. (2017a). The evolution of
597 springtime water vapor over Beijing observed by a high dynamic Raman lidar
598 system: case studies. *IEEE Journal of Selected Topics in Applied Earth*
599 *Observations and Remote Sensing*, *10*(5), 1715–1726.
600 https://doi.org/10.1109/JSTARS.2017.2653811

601 Su, T., Li, J., Li, C. C., Xiang, P. Z., Lau, A. K. H., Guo, J. P., … & Miao, Y. C.
602 (2017b). An intercomparison of long-term planetary boundary layer heights
603 retrieved from CALIPSO, ground-based lidar, and radiosonde measurements over
604 Hong Kong. *Journal of Geophysical Research: Atmospheres*, *122*, 3929–3943.
605 https://doi.org/10.1002/2016JD025937

606 Su, T., Li, Z., & Kahn, R. (2018). Relationships between the planetary boundary layer
607 height and surface pollutants derived from lidar observations over China: regional
608 pattern and influencing factors. *Atmospheric Chemistry and Physics*, *18*(21),
609 15,921–15,935. https://doi.org/10.5194/acp-18-15921-2018

610 Su, T., Li, Z., & Kahn, R. (2020). A new method to retrieve the diurnal variability of
611 planetary boundary layer height from lidar under different thermodynamic
612 stability conditions. *Remote Sensing of Environment*, *237*, 111519.
613 https://doi.org/10.1016/j.rse.2019.111519

614 Teixeira, J., & Hogan, T. F. (2002). Boundary layer clouds in a global atmospheric
615 model: simple cloud cover parameterizations. *Journal of Climate*, *15*(11),

https://doi.org/10.5194/acp-2021-302
Preprint. Discussion started: 1 July 2021

1261–1276. https://doi.org/10.1175/1520-0442(2002)015<1261:BLCIAG>2.0.CO;Vogelezang, D. H. P., and Holtslag, A. A. M. (1996). Evaluation and model impacts of alternative boundary-layer height formulations. *Boundary-Layer Meteorology*, *81*(3-4), 245–269. https://doi.org/10.1007/BF02430331

Wallace, J. M., & Hobbs, P. V. (2006). *Atmospheric Science: an Introductory Survey*. Amsterdam, Boston: Elsevier Academic Press.

Warren, G., Hahn, C. J., London, J., Chervin, M., & Jenne, R. L. (1986). Global distribution of total cloud cover and cloud type amounts over land. (Rep. DOE/ER-0406). Washington, DC: U.S. DOE Office of Energy Research.

Wei, J., Huang, W., Li, Z., Sun, L., Zhu, X., Yuan, Q., Liu, L. and Cribb, M., 2020. Cloud detection for Landsat imagery by combining the random forest and superpixels extracted via energy-driven sampling segmentation approaches. Remote Sensing of Environment, 248, p.112005.

Welton, E. J., Campbell, J. R., Spinhirne, J. D., & Scott III, V. S. (2001). Global monitoring of clouds and aerosols using a network of micropulse lidar systems. In *Lidar Remote Sensing for Industry and Environment Monitoring* (Vol. 4153, 151–158). International Society for Optics and Photonics.

Wu, X., Grabowski, W. W, & Moncrieff, M. W. (1998). Long-term behavior of cloud systems in TOGA COARE and their interactions with radiative and surface processes. Part I: Two-dimensional modeling study. *Journal of the Atmospheric*

https://doi.org/10.5194/acp-2021-302
Preprint. Discussion started: 1 July 2021


Atmospheric Chemistry and Physics Discussions

637 *Sciences*, *55*(17), 2693–2714.
638 https://doi.org/10.1175/1520-0469(1998)055<2693:LTBOCS>2.0.CO;2

639 Yang, D., Li, C., Lau, A. K. H., & Li, Y. (2013). Long-term measurement of daytime
640 atmospheric mixing layer height over Hong Kong. *Journal of Geophysical*
641 *Research: Atmospheres*, *118*(5), 2422–2433. https://doi.org/10.1002/jgrd.50251

642 Yang, T., Wang, Z., Zhang, W., Gbaguidi, A., Sugimoto, N., Wang, X., Matsui, I. and
643 Sun, Y., 2017. Boundary layer height determination from lidar for improving air
644 pollution episode modeling: development of new algorithm and evaluation.
645 Atmospheric Chemistry and Physics, 17(10), p.6215.

646 Zhao, C., Wang, Y., Wang, Q., Li, Z., Wang, Z., & Liu, D. (2014). A new cloud and
647 aerosol layer detection method based on micropulse lidar measurements. *Journal*
648 *of Geophysical Research: Atmospheres*, *119*(11), 6788–6802.
649 https://doi.org/10.1002/2014JD021760

650 Zheng, Y., & Li, Z. (2019). Episodes of warm-air advection causing cloud-surface
651 decoupling during the MARCUS. *Journal of Geophysical Research: Atmospheres*,
652 *124*(22). https://doi.org/10.1029/2019JD030835

653 Zheng, Y., & Rosenfeld, D. (2015). Linear relation between convective cloud base
654 height and updrafts and application to satellite retrievals. *Geophysical Research*
655 *Letters*, *42*(15), 6485–6491. https://doi.org/10.1002/2015GL064809

656 Zheng, Y., Rosenfeld, D., & Li, Z. (2018). Estimating the decoupling degree of
657 subtropical marine stratocumulus decks from satellite. *Geophysical Research*

https://doi.org/10.5194/acp-2021-302
Preprint. Discussion started: 1 July 2021

Atmospheric Chemistry and Physics Discussions

Letters, *45*. https://doi.org/10.1029/2018GL078382

Zheng, Y., Sakradzija, M., Lee, S.-S., & Li, Z. (2020). Theoretical understanding of the linear relationship between convective updrafts and cloud-base height for shallow cumulus clouds. Part II: Continental conditions. *Journal of the Atmospheric Sciences*, *77*, 1313–1328. https://doi.org/10.1175/JAS-D-19-0301.1

https://doi.org/10.5194/acp-2021-302
Preprint. Discussion started: 1 July 2021

Atmospheric Chemistry and Physics Discussions

663 **Tables**

664 **Table 1.** List of parameters in the flow chart of DTDS (Figure 5). These parameters
665 are related with three factors, including LCL, PBLH, CBH. The sensitivity of
666 selection of these parameters is presented. The detailed impacts of variations in these
667 parameters on the retrievals of cloud coupling and PBLH are presented in Figure 7
668 and Figure 8, respectively.

669

670

	Unit	Related factors	Value	Sensitivity (coupled states)	Sensitivity (PBLH)
A_1	km	LCL / PBLH	0.7	Low	Low
A_2	km	PBLH	0.2	**High**	Low
A_3	km	LCL	0.15	Low	Low
A_4	dimensionless	CBH	1.35	Low	Low
A_5	dimensionless	CBH	1.1	Low	**High**

https://doi.org/10.5194/acp-2021-302
Preprint. Discussion started: 1 July 2021

671 **Figures**

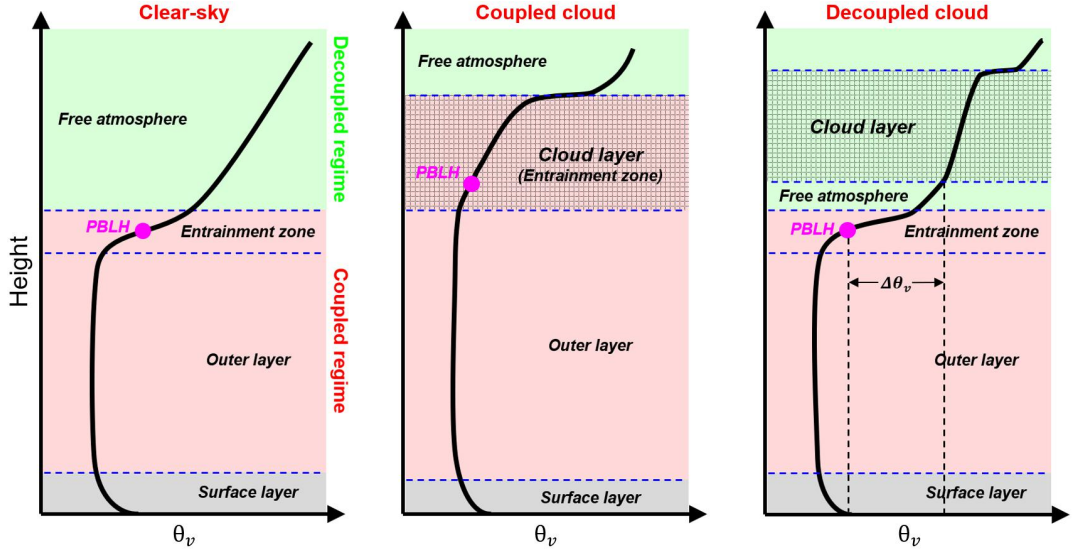

672

673 **Figure 1.** Idealized vertical profiles of virtual potential temperature (θ_v) under the
674 clear-sky, coupled cloud, and decoupled cloud over land. The surface layer, outer
675 layer entrainment zone, and free atmosphere are divided by the blue dash lines. The
676 cloudy layer is marked as the shaded area, and PBLH is marked as the pink point. Red
677 and green zones indicate the coupled and decoupled regime, respectively. Elements
678 (e.g., turbulence, heat fluxes, cloud) in the coupled regime are directly affected by the
679 PBL processes, while these elements are not directly affected by the PBL processes in
680 the decoupled regime. For the coupled cases, the cloud base is below the capping
681 inversion of entrainment zone. For the decoupled cases, the cloud base is above the
682 capping inversion.

683

684

https://doi.org/10.5194/acp-2021-302
Preprint. Discussion started: 1 July 2021

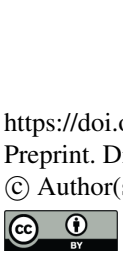

Atmospheric Chemistry and Physics Discussions

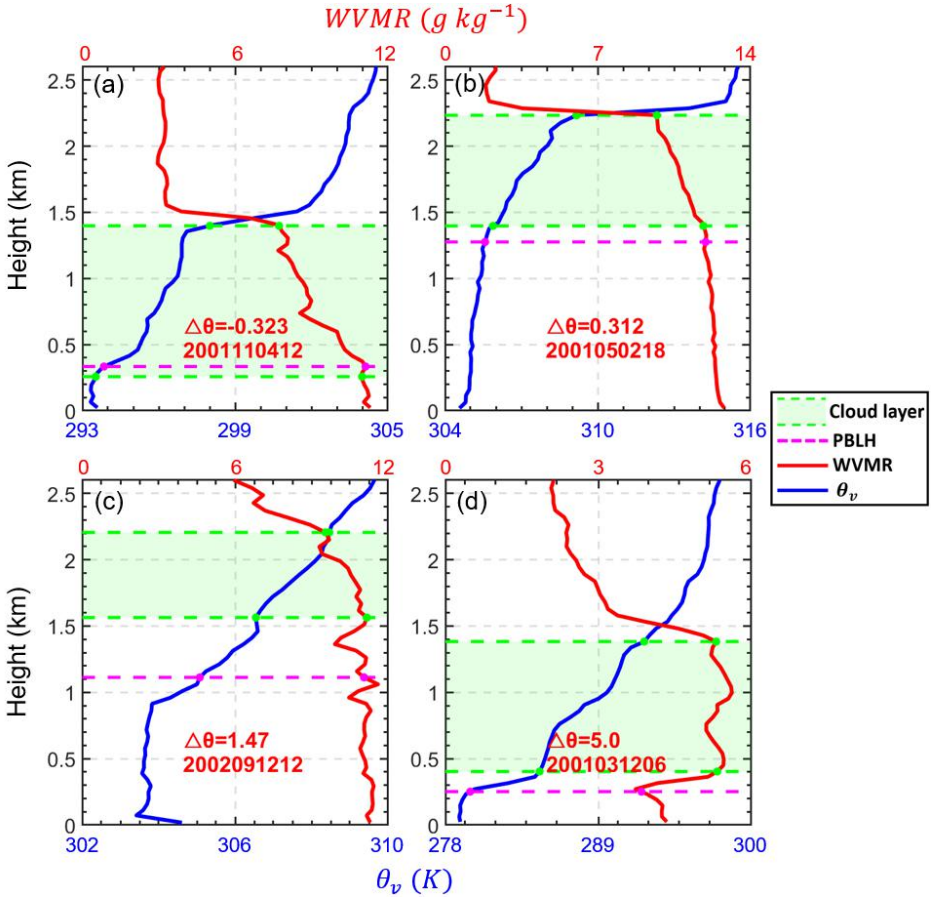

685

686 **Figure 2.** Virtual potential temperature (θ_v, red lines) and water vapor mixing ratio
687 (WVMR, blue lines) profiles from radiosonde (RS) over the Southern Great Plains
688 site for different cases. The differences in virtual potential temperature between the
689 cloud base and the planetary boundary layer (PBL) top are expressed as $\Delta\theta_v$ ($\theta_v^{CBH} -$
690 θ_v^{PBLH}) . The time of each radiosonde launch is marked in each panel as
691 "YYYYMMDDHH", where YYYY, MM, DD, and HH indicates the year, month, day,
692 and local time, respectively. Green regions are cloud layers, and green dashed lines
693 indicate their boundaries. PBL heights are marked as dashed pink lines.

https://doi.org/10.5194/acp-2021-302
Preprint. Discussion started: 1 July 2021

Atmospheric Chemistry and Physics Discussions

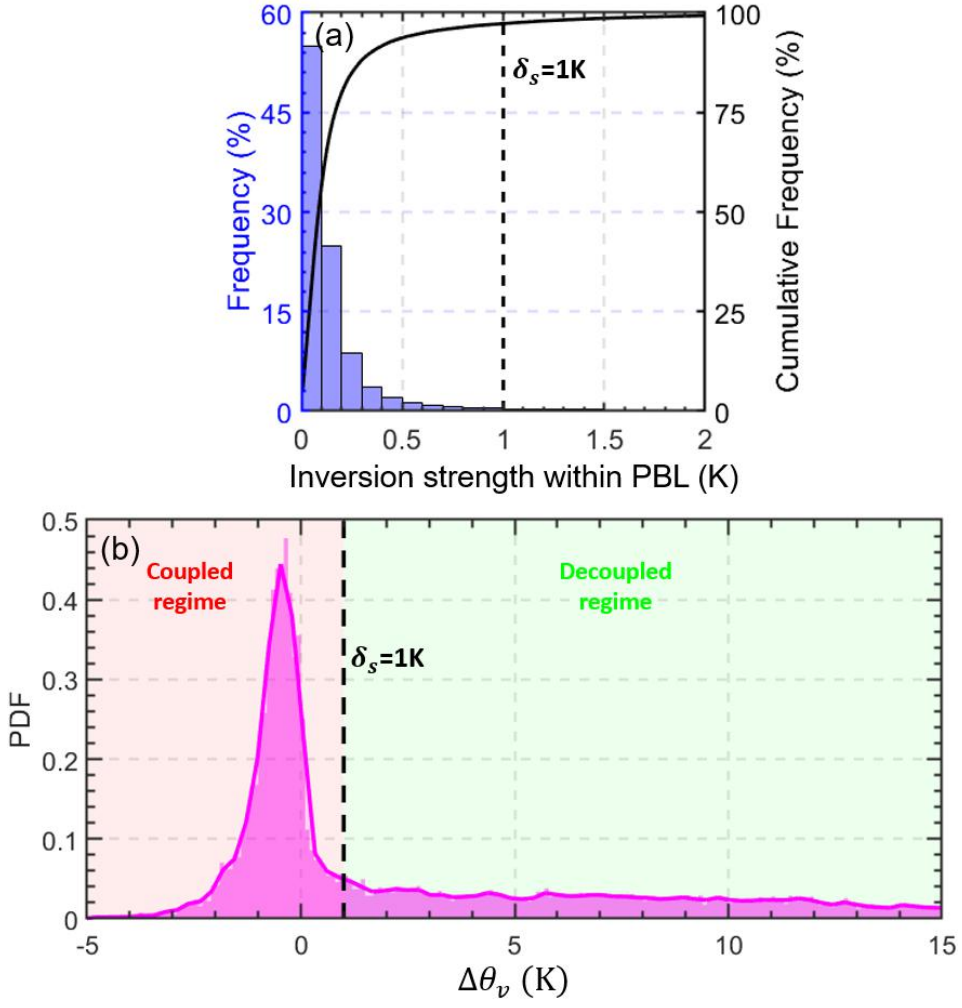

694

695 **Figure 3.** (a) Blue bars represent the inversion strength of θ_v within the PBL. The
696 inversion strength is derived from the radiosonde during daytime (0800-1900LT). The
697 inversions near surface or across PBL top are excluded. The black solid line
698 represents cumulative frequency. (b) Pink area represents the probability density
699 function (PDF) of the differences in the virtual potential temperature between
700 cloud-base height (CBH) and PBLH ($\Delta\theta_v = \theta_v^{CBH} - \theta_v^{PBLH}$). By using a threshold of
701 δ_s (1 K), coupled and decoupled regimes are classified.

https://doi.org/10.5194/acp-2021-302
Preprint. Discussion started: 1 July 2021

Atmospheric Chemistry and Physics Discussions

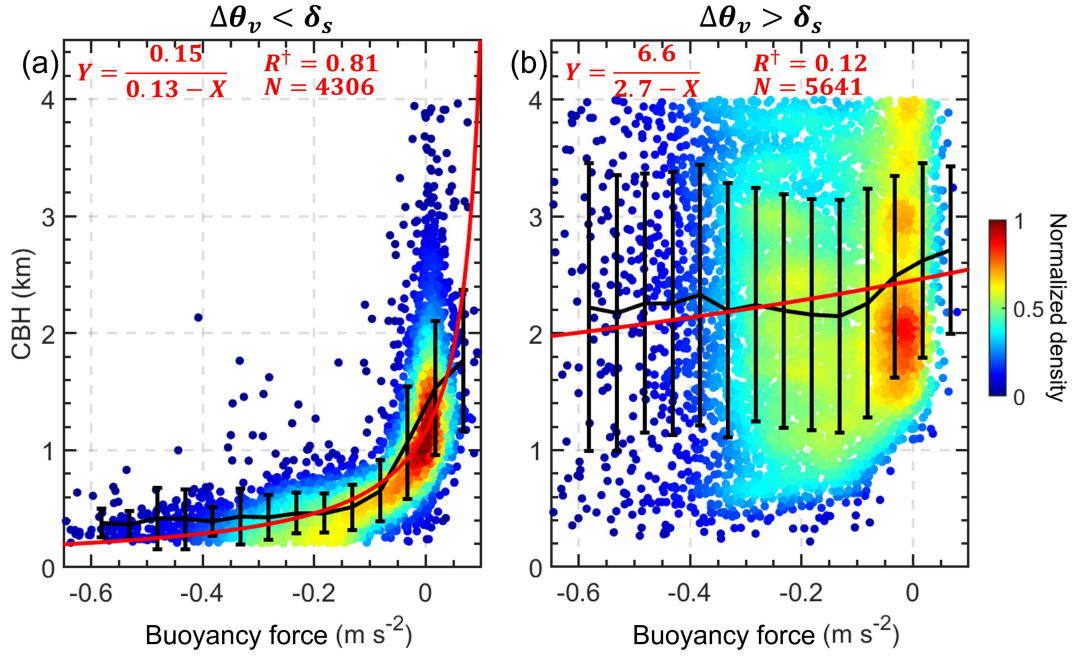

Figure 4. The relationships between cloud-base height (CBH) and buoyancy forces in the lower atmosphere (0–1 km) for (a) $\Delta\theta_v < \delta_s$ and (b) $\Delta\theta_v > \delta_s$. $\Delta\theta_v$ represents the differences in the virtual potential temperature (θ_v) between CBH and PBLH. Black lines represent the mean values in each bin, and the whiskers indicate the standard deviations. Red lines represent the inverse fits. The fitting functions and number of samples (N) are given in each panel, along with the correlation coefficient ($R^{\dagger}$) for the inverse fit.

https://doi.org/10.5194/acp-2021-302
Preprint. Discussion started: 1 July 2021

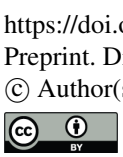

Atmospheric Chemistry and Physics Discussions

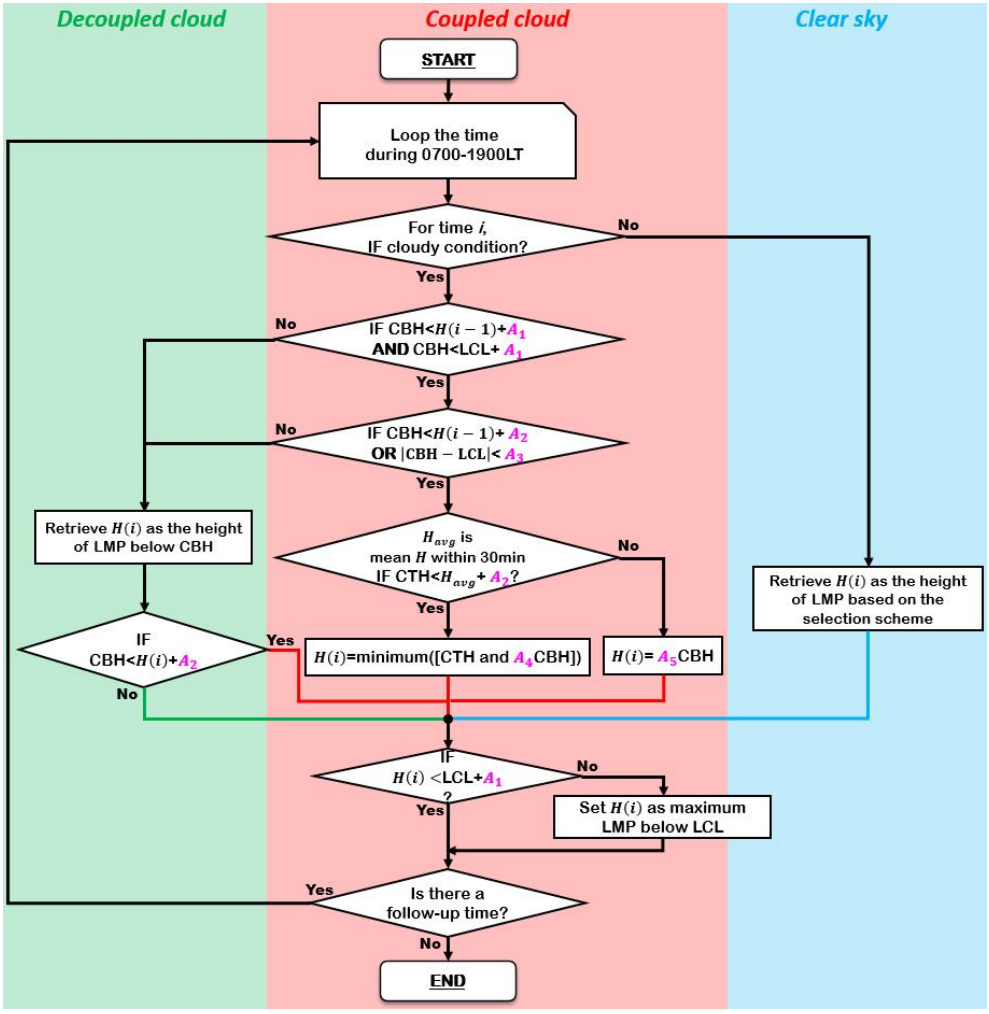

Figure 5. The flow chart of the updated DTDS algorithm. In this diagram, $H(i)$ is the retrieved planetary boundary layer height (PBLH) at time i. CBH and CTH represent the base and top heights, respectively, of the lowest cloud at time i. The PBLH part for selecting the suitable local maximum position (LMP) follows Su et al. (2020), and a detailed scheme for identifying a coupled cloud is added to the DTDS algorithm. LCL stands for lifted condensation level. Five empirical parameters (A_1, A_2, A_3, A_4, A_5) are set as 0.7, 0.2, 0.15, 1.35, 1.1, respectively.

https://doi.org/10.5194/acp-2021-302
Preprint. Discussion started: 1 July 2021

Atmospheric Chemistry and Physics Discussions

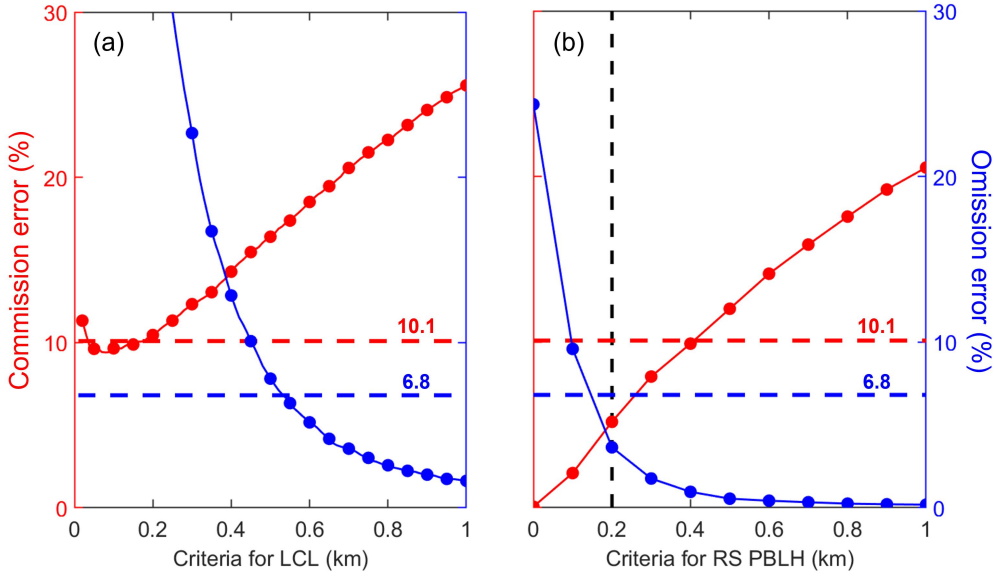

718

719 **Figure 6.** Commission errors and omission errors of coupled cloud identifications (a)
720 for different criteria for the lifted condensation level (LCL) and (b) for different
721 criteria for the planetary boundary layer height (PBLH). "Criteria for LCL" means
722 coupled clouds are identified if $|\mathrm{CBH} - \mathrm{LCL}| <$ Criteria for LCL. Similarly, "Criteria
723 for RS PBLH" means coupled clouds are identified if $\mathrm{CBH} - \mathrm{RS\ PBLH} <$ Criteria
724 for RS PBLH. The red and blue dashed lines indicate the commission and omission
725 errors, respectively, for the DTDS algorithm. CBH stands for cloud-base height, and
726 RS stands for radiosonde.

727

728

729

730

https://doi.org/10.5194/acp-2021-302
Preprint. Discussion started: 1 July 2021

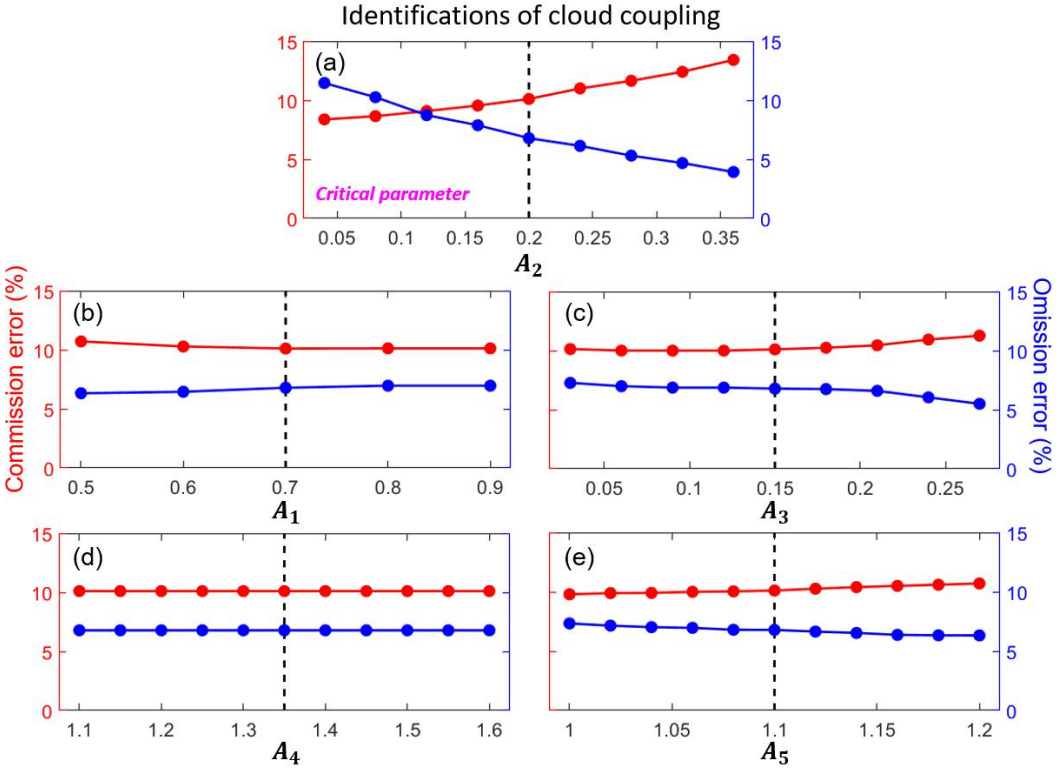

731

732 **Figure 7.** Commission errors (red line) and omission errors (blue line) of coupled
733 cloud identifications for selecting different values of empirical parameters
734 (A_1, A_2, A_3, A_4, A_5) in the DTDS algorithm. Black dash lines indicate the default
735 values. For each test, one parameter is variable, while other parameters are set as
736 default values. For identifications of cloud coupling, A_2 is the critical parameter.

https://doi.org/10.5194/acp-2021-302
Preprint. Discussion started: 1 July 2021

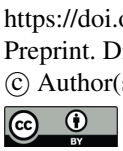

Atmospheric Chemistry and Physics Discussions

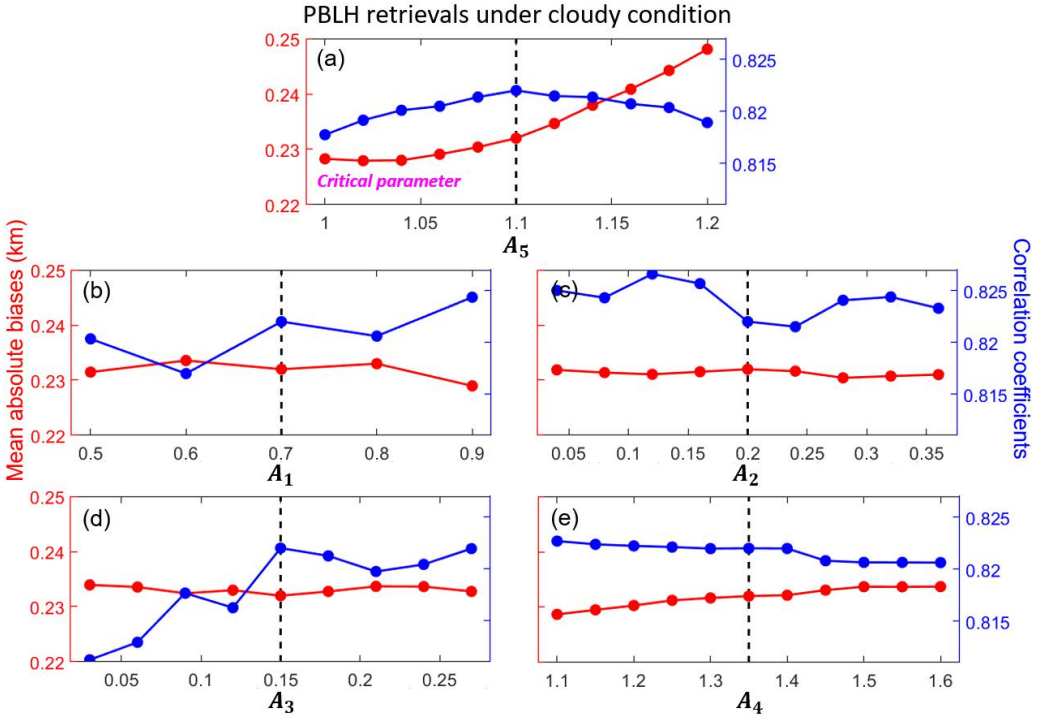

Figure 8. Red lines indicate the mean absolute biases between PBLH derived from lidar and radiosonde for selecting different values of empirical parameters (A_1, A_2, A_3, A_4, A_5) in the DTDS algorithm. Here, we only analyze the low cloud cases. Blue lines indicate the corresponding correlation coefficients between PBLH derived from lidar and radiosonde. Black dash lines indicate the default values. For each test, one parameter is variable, while other parameters are set as default values. For PBLH retrievals under cloudy conditions, A_5 is the critical parameter.

https://doi.org/10.5194/acp-2021-302
Preprint. Discussion started: 1 July 2021

Atmospheric Chemistry and Physics Discussions

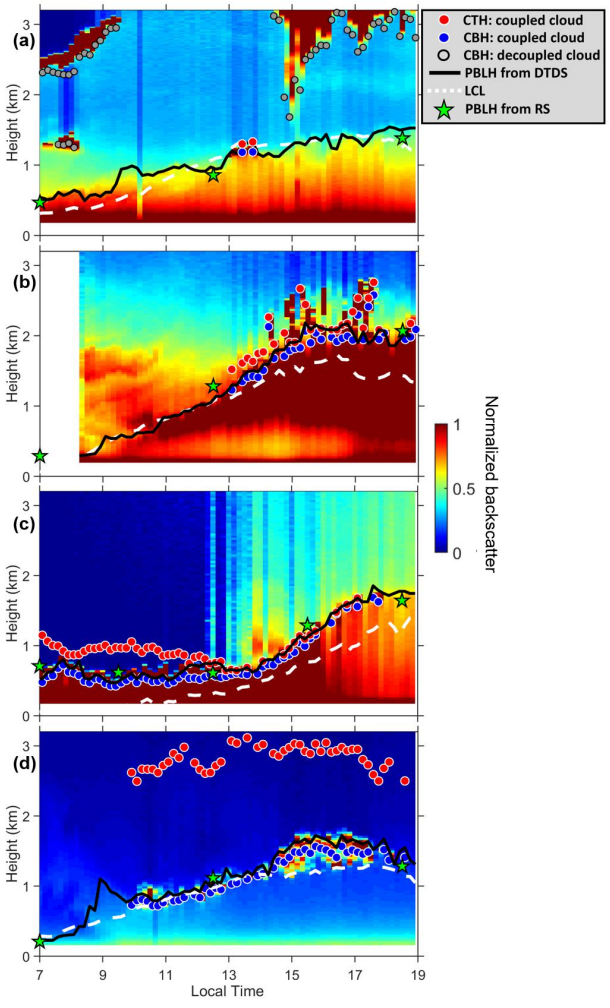

745

746 **Figure 9.** Daily backscatter profiles: (a) short-lived coupled cloud, (b) developed
747 coupled cloud, (c) daylong coupled cloud, and (d) active coupled cloud. Backscatter is
748 normalized to a range of 0–1 in arbitrary units. Red dots and blue dots indicate
749 cloud-top heights (CTHs) and cloud-base heights (CBHs) of coupled clouds. Grey
750 dots mark CBHs for decoupled clouds. Black lines and green stars mark the planetary
751 boundary layer height (PBLH) retrieved from the DTDS algorithm and from
752 radiosonde (RS) soundings, respectively. White dashed lines represent lifted

https://doi.org/10.5194/acp-2021-302
Preprint. Discussion started: 1 July 2021

Atmospheric Chemistry and Physics Discussions

753 condensation levels (LCLs).

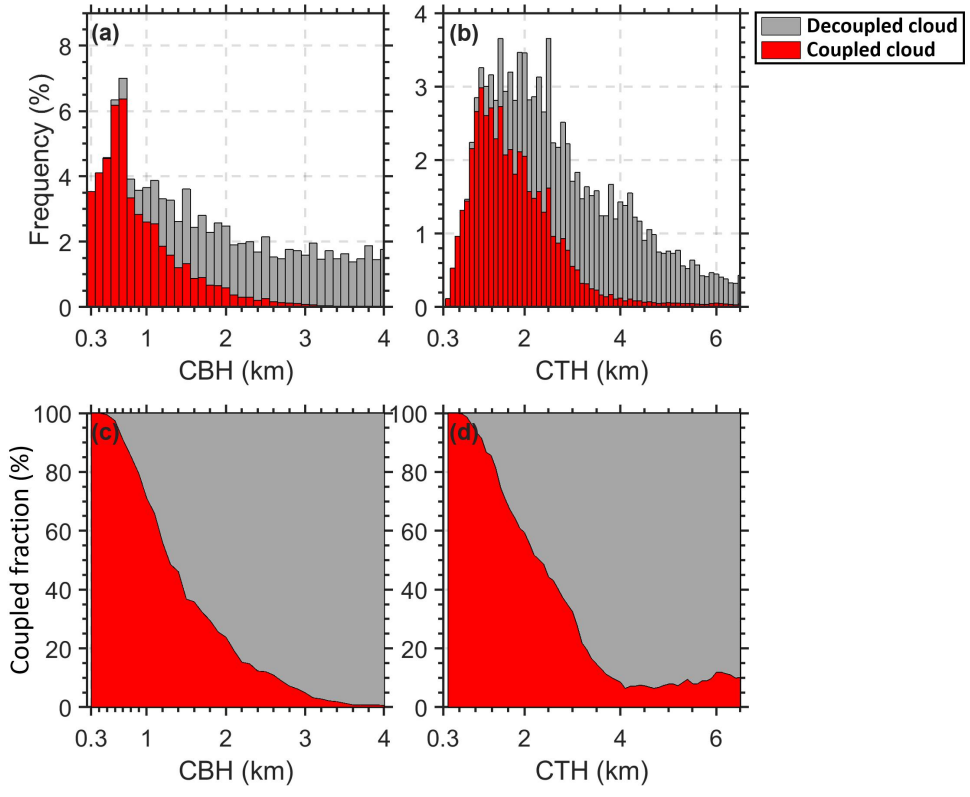

754

755 **Figure 10.** The height-dependent occurrence frequencies of (a) the cloud-base height
756 (CBH) and (b) the cloud-top height (CTH) for coupled clouds (red bars) and
757 decoupled clouds (grey bars). The relative occurrence frequencies of (c) the CBH and
758 (d) the CTH for coupled clouds (red area) and decoupled clouds (grey area).

759

https://doi.org/10.5194/acp-2021-302
Preprint. Discussion started: 1 July 2021

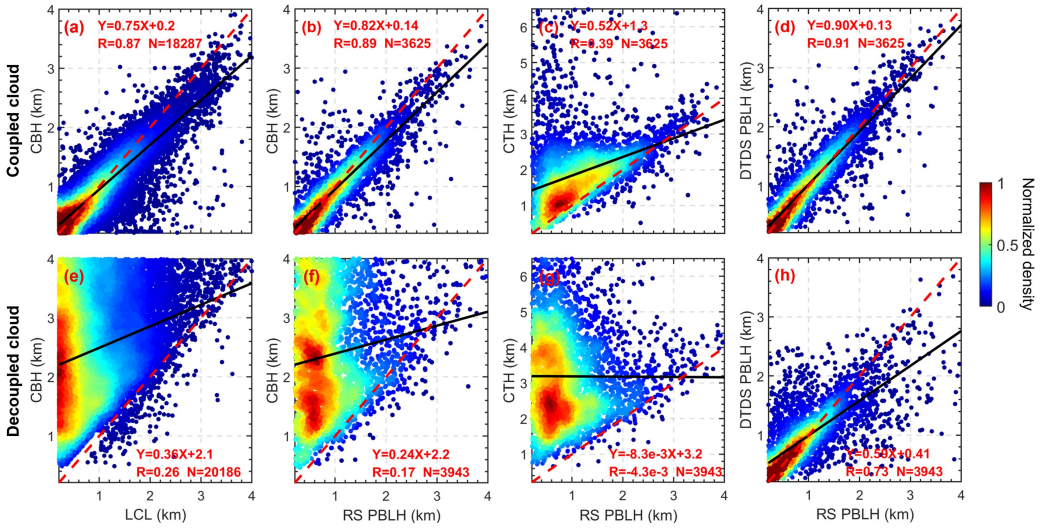

Figure 11. The relationships between (a) LCL and CBH, (b) CBH and RS-derived PBLH, (c) CTH and RS-derived PBLH for coupled clouds, and (d) DTDS-derived PBLH and RS-derived PBLH. Panels (e-h) are similar to panels (a-d) but for decoupled clouds. Black lines represent the linear regressions. The linear fitting functions, correlation coefficients (R), and sampling numbers (N) are given in each panel.